



**Environmental
Science**
Nano

**Coupling Single Particle ICP-MS with Field-flow
Fractionation for Characterizing Metal Nanoparticles
Contained in Nanoplastic Colloids**

Journal:	<i>Environmental Science: Nano</i>
Manuscript ID	EN-ART-06-2019-000637.R2
Article Type:	Paper

SCHOLARONE™
Manuscripts

Environmental Significance Statement

There remains uncertainty over the consequences of introducing engineered nanoparticles (ENPs) and nanoplastics into the environment. Partial transformations can occur in the environment that lead to complex composite colloids that can contain ENPs, organic matter, and/or MPs. The physical form of ENPs released during the use and disposal phases will likely influence their environmental fate and impact. We have developed a methodology that uses multiple means of nanoparticle characterization to provide a clearer picture of the physical properties (i.e. size, number of incorporated components) of composite particles. While at the proof of concept phase, continued refinement of the methodology will allow application for investigating ENP properties in environmental systems and to use of embedding metal NPs into nanoplastics in order to track their environmental transformations.

Coupling Single Particle ICP-MS with Field-flow Fractionation for Characterizing Metal Nanoparticles Contained in Nanoplastic Colloids

Angela Barber^{1,3}, Sun Kly², Matthew G. Moffitt², Logan Rand¹, and James F. Ranville^{1*}

¹Department of Chemistry, Colorado School of Mines, Golden, CO, 80403

²Department of Chemistry, University of Victoria, Victoria, B.C. V8W 2Y2

³Arcadis U.S., Inc., Broomfield, CO, 80021

KEYWORDS: *Centrifugal FFF, AF4, polymer nanocomposite, nanotechnology, heteroaggregates*

ABSTRACT: Use of nano-enabled products increases the potential for release of engineered nanoparticles (ENP) into the environment. Product weathering and further environmental transformations can create composite particles (CPs) that may contain multiple ENPs, a residual product matrix (e.g. polymer), or transformed/added surface coatings. Methodology that uses transmission electron microscopy (TEM), single particle ICP-MS (spICP-MS) and field-flow fractionation (FFF) was developed to facilitate the investigation of metallic ENPs associated with CPs. In this study, colloidal-sized nanoplastic CPs consisting of gold-polymer nanocomposite (polystyrene-*block*-poly(acrylic acid)) were examined to reveal how combining FFF with spICP-MS can be used to characterize CPs. Metal NP size and particle number concentration is obtained by spICP-MS. Asymmetric flow field-flow fractionation (AF4) and centrifugal field-flow fractionation (CFFF) separate and size the CPs based on their hydrodynamic diameter and buoyant mass, respectively. Off-line spICP-MS analysis of fractions obtained by the FFF separations facilitated measurement of the mass and number of Au-PS (gold-polystyrene) ENPs (from 1 to >8) contained in the CPs. In particular, CFFF utilizing a carrier that was density-matched to the polymer proved very successful in measuring multiple gold ENPS in the CPs. The developed methodology can be applied to investigate ENP properties in environmental systems.

INTRODUCTION

The uncertainty over the possible consequences of introducing engineered nanoparticles (ENPs) and microplastics (1-5000 μm in size) into the environment is a driver to develop new analytical methods for their characterization. ENPs are incorporated into nanotechnology-enabled products in order to provide a desired function, resulting in large societal benefits¹. Products containing metallic ENPs are increasingly being utilized in disinfection/water treatment², medicine³, and materials science⁴. Predicting the risks posed to human health and the environment by nanomaterials is difficult due to challenges in quantifying exposure parameters (e.g., release rates, transport, stability, and fate). Among the unknowns is the form of released ENPs. Partial ENP transformations can occur in the environment through surface modification (i.e. formation and alteration of coatings), hetero-aggregation with natural particles, and partial chemical degradation (e.g. surface oxidation or sulfidation)⁵⁻⁶. Environmental samples may therefore commonly contain ENPs existing in a complex composite structure (i.e. multielement, multiphase). Similarly, the key role plastics play in society has led to the environmental release of microplastics, which degrade to nanoplastics (1-1000 nm)⁷. It has been recently proposed that the environmental behavior of model micro- and nano-plastics could be better examined in treatment systems by introducing metals into the polymer to provide an elemental tracer⁸. Using well-defined, monodisperse metal NPs could be similarly useful, with the added benefit that each NP has a well-known elemental mass. Embedding even a single nanoparticle into each nanoplastic particle can introduce a substantial number of metal ions that could be used to track processes in experimental systems (laboratory, mesocosm, or full-scale treatment plants). The potential presence of ENPs in environmental systems demonstrates a clear need for continued advancements in nanometrology capable of analyzing increasingly complex materials⁹⁻¹¹

1 This study focused on new combinations of analytical approaches capable of characterizing
2 composite particles (CPs) that contain both metallic and organic (polymeric) phases, which can
3 represent ENP-containing materials likely to be found in the environment. Protein coronas formed on
4 ENPs during biological interaction/uptake¹²⁻¹⁴ and nanoplastics (e.g., polymer-NP composites)
5 generated by weathering of nano-enabled products are examples¹⁵. In this latter case the fragments
6 could retain metal NPs and some of the polymer matrix. In a prior study of carbon nanotube release
7 from a polymer composite we measured yttrium, present as residual catalyst NPs, to show
8 weathering-generated fragments, in the form of nanoplastics, having a structure consisting of carbon
9 nanotube bundles incorporated inside a polymer residue¹⁶. In environmental systems, CPs having both
10 organic and inorganic components are also likely to be created due to the ubiquity of natural background
11 mineral particles, dissolved organic matter (i.e., humic substances), and biomolecules. In this study Au
12 NPs contained in polymer core/shell colloids were prepared and characterized to represent these CP
13 types.
14
15
16
17
18
19
20
21
22
23
24
25
26
27
28
29

30 The development of new nanometrology to quantify (mass and/or number concentration) and
31 characterize (size, composition, structure, aggregation state) colloids, including ENPs, is essential to
32 assessing the impacts of their release¹⁷. Quantitative characterization of complex CPs by traditional
33 nanometrology techniques, such as transmission electron microscopy (TEM) and dynamic light
34 scattering (DLS), is often challenging and prone to artifacts^{18,19}. To address this issue, we present an
35 analytical methodology using single particle ICP-MS (spICP-MS) applied following a separation step,
36 in this case field-flow fractionation (FFF). This combination of techniques is a highly promising
37 alternative and/or addition to the traditional techniques to more fully characterize CPs. The methods
38 can provide the total CP size, the mass (and number) of NPs per CP, and the thickness of the
39 organic/polymer coating. Analysis by spICP-MS provides the particle number concentration and the
40 inorganic NP size, which is based on elemental mass²⁰⁻²³. Asymmetrical flow field-flow fractionation
41
42
43
44
45
46
47
48
49
50
51
52
53
54
55
56
57
58
59
60

(AF4) and centrifugal FFF (CFFF) separate the sample constituents based on their hydrodynamic size and buoyant mass, respectively^{24,25}. FFF theory or size calibration can be used to compute particle size.

The first study objective was to compare the techniques of TEM, spICP-MS, AF4, and CFFF for measuring mean size and size distribution width of monodisperse ENPs. A key parameter obtained by the spICP-MS methodology is the particle size distribution width, as this measurement can be a sensitive indicator of aggregation. The second objective was to demonstrate the quantitative capabilities of spICP-MS for characterizing CPs that may contain multiple NPs. We demonstrate that for model systems, increased size distribution width determined by spICP-MS can show the presence of CPs containing multiple metal NPs. The third objective of this study was to determine the distribution of metal NPs incorporated in CPs as size or buoyant mass increases. We show: 1.) FFF provides information on how metal NP mass is distributed across the size distribution, which for model systems can be a consequence of incorporation of multiple NPs, 2.) when spICP-MS is combined with AF4, the presence of organic matter components of the CPs can be assessed, and 3.) CFFF can provide separation of CPs by the mass, and for model systems, number of metal NPs contained therein. The methodologies developed in this project overcomes some key limitations in other techniques, and has potential use in industrial manufacturing processes, monitoring release of ENPs and MPs into the environment, and assessing abiotic and biologically-mediated transformations of these materials.

MATERIALS AND METHODS

Model Composite Particle Synthesis. The model CP used was a polymer nanocomposite (Au-PS/PS-*b*-PAA) that could contain none, one, or many polystyrene brush-coated Au NPs (Au-PS) (Figure 1), which were first prepared by coating Au-citrate NPs (Au-cit, approximately 40-50 nm in diameter). Water-dispersible CPs were created using amphiphilic block copolymer polystyrene-block-poly(acrylic acid) (PS-*b*-PAA) chains, which form a coating up to about 200 nm thick (Figure 1). Dispersions of Au-

1 PS/PS-*b*-PAA CPs were prepared by microprecipitation of Au-PS NPs and the amphiphilic block
2 copolymer PS-*b*-PAA dispersed in dimethylformamide via mixing with water in a two-phase gas-liquid
3 microfluidic reactor. Details of the microfluidic reactor and its application to producing polymer-
4 inorganic CPs can be found in previous publications ²⁶⁻²⁹. Specific details of the synthesis of both the
5 Au-PS NP and the CP are provided in the ESI (ESI-1 and ESI-2).
6
7
8
9
10

11 **Characterization Methods.** The three particle types (Au-cit, Au-PS, and Au-PS/PS-*b*-PAA
12 CPs) were analyzed by spICP-MS, AF4, CFFF, and TEM. Total ¹⁹⁷Au concentrations of the solutions
13 containing Au-cit NP and Au-PS/PS-*b*-PAA CP colloids (1:1000 dilution in Milli-Q water) were
14 measured by ICP-MS (Perkin Elmer NexION 300D) using a dwell time of 2.19 seconds (matching
15 AF4-UV-vis data collection frequency) with 55 total readings and a 1 mL/min sample flow rate.
16 Calibration was performed using 0, 1, 10, and 100 µg/L dissolved Au (SPEX CertiPrep) in 2% (v/v)
17 HCl (Figure ESI-1).
18
19
20
21
22
23
24
25
26
27

28 TEM imaging of the Au-PS NPs and the Au-PS/PS-*b*-PAA CPs was conducted using Jeol JEM
29 1400 operated at 80 keV. Samples were dropped onto CF300-Cu Carbon film mesh copper grids from
30 deionized water and whisked dry after 30 seconds. To minimize beam damage, low electron voltages
31 were used and images were collected with a bottom-mounted Gatan SC200 CCD camera. ImageJ™
32 image analysis software was used to evaluate particle distributions.
33
34
35
36
37
38
39

40 The Au-cit NPs and the Au-PS/PS-*b*-PAA CPs were also analyzed by spICP-MS. Additionally,
41 during separation of the Au-PS/PS-*b*-PAA CPs by AF4 and CFFF, selected fractions of the eluent were
42 collected, diluted, and analyzed by spICP-MS. Analyses were performed using 100 microsecond (µs)
43 dwell times, no settling time, and a very short detector dead time (35 ns) between readings³⁰⁻³².
44 Additional acquisition conditions and a summary of all spICP-MS analyses performed are shown in the
45 ESI (Table ESI-1, ESI-2). Data acquisition and data processing were performed using a pre-release
46 version of the Syngistix™ Nano Application Module provided to the authors by Perkin Elmer. A 60 nm
47
48
49
50
51
52
53
54
55
56
57
58
59
60

1 Au NP (NIST SRM 8013) and dissolved Au standards were used to determine spICP-MS transport
2 efficiency following the mass-based procedure of Pace et al.³³ and was typically 6-12%. Particle events
3 were identified as ICP-MS responses above the threshold intensity, determined using the average plus
4 3σ method³⁴. The total intensity of each NP event is determined by summation of all consecutive
5 readings above the threshold, from which the element mass is determined and particle diameter is
6 computed assuming a gold density of 19.3 g/cm³ and a spherical geometry^{34,35}. The particle number
7 concentration is proportional to the number of NP events detected after adjustment for the sample flow
8 rate and transport efficiency.
9

10
11
12
13
14
15
16
17
18
19 A Postnova Analytics AF2000 AT AF4 with online UV-visible (254 and 520 nm wavelengths)
20 and/or ICP-MS detectors was used to separate, by hydrodynamic size, the Au-cit NPs and Au-PS/PS-*b*-
21 PAA CPs. All separations were performed with a cross-flow of 0.5 mL/min and an outlet flow rate of 1
22 mL/min to the detector(s). Other specific details of the FFF separation conditions and the measurement
23 of the percent recovery are provided in the ESI (Table ESI-3). Hydrodynamic diameter was calibrated
24 using dispersions of 0.01% (v/v) PS spheres of 60 nm, 100 nm, and 140 nm (Thermo Scientific) and/or
25 30 nm and 60 nm Au-citrate NPs (NIST, SRM 8012 and SRM 8013, respectively) (each at 1.25-12.5
26 mg/L). Size calibrations were performed at least once each day of AF4 analysis (Figure ESI-2). On-line
27 ICP-MS also provided a continuous fractogram for ¹⁹⁷Au. Several separations of the Au-PS/PS-*b*-PAA
28 CPs are reported, as summarized in Table ESI-3.
29
30
31
32
33
34
35
36
37
38
39
40
41

42 A Postnova Analytics CF2000 CFFF was used to separate and size the Au-cit NPs and the Au-
43 PS/PS-*b*-PAA CPs. For the latter, a carrier solution of 24% (v/v) glycerol and 0.05% (v/v) FL-70 was
44 used. This provided a density of approximately 1.056 g/mL, which closely matched the density of the
45 PS-*b*-PAA shell (assumed to be 1.05 g/cm³). The resulting neutral buoyancy of the polymer coating
46 provided separation by the incorporated Au mass only. A power decay program was used, which
47 provided a non-linear (exponential) relationship between retention time and particle mass (Figure ESI-
48
49
50
51
52
53
54
55
56
57
58
59
60

3c). Thirty fractions (3 minutes duration) were collected, and select fractions were analyzed by spICP-MS. Online UV-vis (Postnova Analytics) at 254 nm and 520 nm and/or 90° light scattering detectors (Postnova Analytics) were used to monitor sample elution. A summary of each separation is provided in the ESI (Table ESI-3). All NP samples, size standards, and FFF fractions were stored at 4°C and diluted in Milli-Q water (18.2 MΩ-cm) each day. Diluted NPs were sonicated for 5 minutes following preparation.

RESULTS AND DISCUSSION

Comparison of Size Analysis Methods for Low-Polydispersity NPs. The size distributions of the Au-cit NPs were determined by spICP-MS, AF4, and CFFF. Incorporation of multiple Au NPs into CPs (e.g. polymer-NP or heteroaggregates) increases both the mean size and the size distribution width (polydispersity) compared to the original Au-PS NP population. In applying spICP-MS to characterize these complex particles using these metrics, it is important to know the comparability to results obtained by other methods. For inorganic, monodisperse particles the most-widely accepted standard for comparison is TEM, which was used to examine the Au-PS NP and the CP. TEM images of the Au-PS NP (Figure 1b,d) show relatively uniform, elongated, sometimes faceted rhomboids, which can be described as pill-shaped particles. The equivalent spherical diameter was computed from the volume obtained by:

$$V = 4/3 \pi(P_t)^3 + \pi(P_d)^2 P_h \quad (1)$$

Where: P_h = length of the cylindrical portion, P_d = short dimension of the cylindrical portion, and P_t = the length of the hemispherical ends of the pill. ImageJ™ particle distribution analysis was applied to 222 particles. The PS coating was not imaged by this method, allowing comparison of the size results to that obtained by other methods for the Au-cit NPs.

Particle size distributions obtained for the Au-Cit and Au-PS (TEM) NPs by the four methods are shown in Figure 2 (a-d). Mass of the Au-cit NPs obtained by spICP-MS was converted to an equivalent spherical diameter using an Au density of 19.5 g/cm³. AF4 and CFFF size distributions were obtained from retention time by calibration. Nanoparticle size distributions were fitted to Gaussian and LogNormal non-linear curve functions using OriginPro 2018™. The fitting parameters μ (mean size) and σ (distribution width) along with their respective standard error reported by the software are shown in Table 1. The error is a measure overall fit of the data by the gaussian and log normal models.

Table 1. Gaussian and Log-Normal fitting statistics of size distributions for Au-PS NP size determined via TEM and Au-cit NP determined by spICP-MS, AF4, and CFFF. Degrees of freedom (DF) represent the number of histogram bins.

Equivalent spherical diameter (nm)		TEM		spICP-MS		AF4		CFFF	
		value	error	value	error	value	error	value	error
Gaussian	μ	46.8	0.52	39.8	0.13	45.4	0.04	41.4	0.02
	σ	7.0	0.82	6.4	0.19	7.3	0.04	4.6	0.02
	DF	17		49		298		702	
	RSS	0.215		0.106		0.193		0.715	
Log Normal	μ	47.6	0.62	40.7	0.20	46.4	0.03	41.8	0.03
	σ	7.2	0.94	6.4	0.31	7.7	0.03	4.6	0.04
	DF	17		49		298		702	
	RSS	0.210		0.215		0.082		1.83	

In the comparison of the four different particle sizing methods, all Gaussian and LogNormal models report similar μ and σ values as well as error (adjusted r^2) for the particle size distributions. The Au-cit NP distribution width obtained by spICP-MS is consistent with TEM results; however, the mean diameter calculated by TEM is about 15% greater than the spICP-MS diameter. AF4-ICP-MS and CFFF-UV-vis results are more consistent with the spICP-MS results. When comparing all four of the

1 methods, mean sizes were in agreement of the overall mean to within approximately 10% regardless of
 2 the distribution model used. The residual sum of squares is minimized slightly more by the Gaussian
 3 model for spICP-MS and the LogNormal model for the AF4 data. CFFF gave a narrower distribution
 4 than those found using the other methods. CFFF, being a mass separation (r^3 function), is often
 5 considered to give higher resolution than AF4 (r function), but it is unclear if this explains the observed
 6 narrower distribution. The CFFF data also did not seem to fit either model well, as shown by the higher
 7 residual sum of squares. These results support the hypothesis that the distribution width obtained by
 8 spICP-MS is comparable to TEM and that this measurand can be used to examine the characteristics of
 9 the CPs generated in this study. Additional comparisons of spICP-MS and TEM (Figure ESI-4) were
 10 made for other NP reference materials (NIST RM 8013, Nanocomposix NPs) or varying distribution
 11 width. The result further support the observation that TEM and spICP-MS give comparable distribution
 12 widths.
 13
 14
 15
 16
 17
 18
 19
 20
 21
 22
 23
 24
 25
 26
 27

28 **Table 2.** Gaussian and Log Normal fitting statistics on Au-cit NP and Au-PS-*b*-PAA NP mass
 29 distributions. Degrees of freedom (DF) represent the number of mass bins.
 30
 31
 32

Mass in $\mu\text{g Au} \times 10^{-9}$		Au-Citrate Mass		Au-PS- <i>b</i> -PAA Mass	
		value	standard error	value	standard error
Gaussian	μ	0.71	0.01	1.53	0.02
	σ	0.30	0.01	0.52	0.02
	DF	46		198	
	RSS	0.193		1.319	
Log Normal	μ	0.84	0.024	1.81	0.02
	σ	0.41	0.032	0.79	0.02
	DF	46		198	
	RSS	0.213		0.554	

Characterization of CPs by spICP-MS Analysis. TEM analysis of the CPs shows Au-PS NPs incorporated inside the larger CPs (Figure 1d). A wide variation in the number of Au NPs per CP was observed by TEM image processing (ImageJ™). Many polymer particles were observed to contain no Au NPs, but for those that did contain Au NPs, almost 50% contained only one Au NP, about 30% contained two or three Au NPs, and the remaining 20% had four or more Au NPs. However we observed that in some cases it appeared that NP overlap could result in an overestimate of the number of single particles in the CP.

Examining mass distributions obtained by spICP-MS (Figure 3), instead of the size distribution, allows for a clearer analysis of the number of NPs incorporated into the CPs. Mass distributions were fitted to Gaussian and LogNormal non-linear curve functions using OriginPro 2018™. The fitting parameters μ (mean size) and σ (distribution width) along with their respective standard errors reported by the software are shown in Table 2. The mass distribution of the Au-cit NPs is fit slightly better by a Gaussian distribution than a LogNormal distribution (as shown by the residual sum of squares). This is in contrast to the Au-PS/PS-*b*-PAA CPs, which are much more closely fit by a LogNormal mass distribution. The skewed Au mass (size) distribution clearly indicates incorporation of multiple Au-PS NPs into the CPs, as was visually observed by TEM. The mean Au mass (1.53×10^{-9} $\mu\text{g Au}$) is slightly larger than twice that of the Au-PS mass (0.71×10^{-9} $\mu\text{g Au}$). This result suggests that most CPs contain 2 NPs with 1 and 3 NPs being the next most common. The discrepancy between this spICP-MS and the TEM result may be attributed to a bias resulting from the overlap of multiple three-dimensional Au NPs in the two-dimensional TEM images, along with poorer counting statistics by TEM.

Using multiples of the Au-cit NP mode mass, it can be seen that the tail of the distribution indicates CPs contain progressively fewer multiple NPs up to approximately 10 NPs. Addition of two FFF techniques, AF4 and CFFF, to the spICP-MS and TEM data provides a more complete particle

1 characterization for CPs by coupling CP particle separation based on hydrodynamic size (AF4) or mass
2 (CFFF) with single particle Au NP mass analysis.
3
4

5 **Characterization of CPs by Field-Flow Fractionation w/spICP-MS Analysis.** The Au-
6 PS/PS-*b*-PAA CPs were separated by both AF4 (Figure 4) and CFFF (Figure 5). Analysis by spICP-MS
7 of collected fractions provides mass distributions of Au NPs at various retention times. Comparison of
8 AF4 obtained size to spICP-MS size provides an important characterization result for CPs. For an
9 uncoated Au NP, both methods should give equivalent sizes provided the AF4 operates in normal mode.
10 This FFF separation mode occurs until about 1 micron, above which particles elute in a steric mode²⁴.
11 However the presence of organic coatings will increase the AF4 determined size without affecting the
12 spICP-MS size.
13
14
15
16
17
18
19
20
21
22

23 As CP size increases, an increasingly greater maximum number of Au-PS NPs can be
24 accommodated into the CP. To provide an approximation of the number distribution of Au NPs
25 contained in each CP within each FFF fraction, the spICP-MS mode mass of the Au-cit NPs (Figure 3a)
26 was used to develop simplified stacked bar histograms (Figure 4b and 5b). To produce these stacked bar
27 histograms, the mode mass ($0.71 \times 10^{-9} \mu\text{g Au}$) was multiplied by an integer value of 1 to 8 (Figure ESI-
28 5). The number of particles within the mass range between the midpoints of the integer masses was
29 summed and divided by the total number of particles to determine an approximate Au NP number
30 distribution in each fraction. For example, to find the number of CPs containing the equivalent mass of
31 three Au NPs, the frequency of particles between a mass of $1.86 \times 10^{-9} \mu\text{g}$ and $2.60 \times 10^{-9} \mu\text{g}$ was
32 summed and normalized to the total frequency. This was performed for up to 8 NPs for both the Au-cit
33 NP and Au-PS/PS-*b*-PAA CP spICP-MS data. In this approach we rely on the known size and
34 relatively narrow distribution of the Au-PS NPs as well as the assumption that incorporation of the Au
35 NP into the polymer has not altered its size. This latter point was verified by TEM analysis. With the
36 size distribution of the Au-cit and Au-PS NPs being described as a normal distribution (Table 2),
37
38
39
40
41
42
43
44
45
46
47
48
49
50
51
52
53
54
55

1 multiples of NPs near the mode mass are the most statistically probable cause for a CP to contain
2 increasing amounts of Au-PS NP. Although much less probable, increasing mass can result from
3 incorporation of a greater or a fewer multiples of NPs present at the lower and upper range of the Au-PS
4 distribution respectively. The ability to assign NPs numbers to each fraction is challenged if
5 polydispersity of the NPs is increased, and thus the counting approach is best applied to monodisperse
6 starting NPs.
7
8
9
10
11
12

13
14
15
16 **Asymmetric Flow Field-Flow Fractionation.** The AF4 recovery for Au-cit and Au-PS/PS-*b*-
17 PAA CPs was calculated as the total integrated intensity over the fractogram (Figure 2c and 4a) with a
18 field applied (0.5 mL/min cross-flow) divided by the integrated intensity of the fractogram with no field
19 applied (0 mL/min cross-flow). Total average recovery was 82% and 127%, for Au-cit and Au-PS/PS-*b*-
20 PAA CPs, respectively (Figure ESI-6). These recoveries were considered acceptable, but not ideal. The
21 recoveries indicate possible interaction of the CPs with the membrane. Some CPs appear to be reversibly
22 adsorbed as demonstrated by the peak that elutes after the field is turned off at the end of the
23 fractionation (90 minutes in Figure 4a). Interaction of NPs with the membrane are generally not
24 particle dependent as the surfactant present in the carrier makes the NPs surfaces uniformly charged and
25 sterically-stable. Poor recoveries arise from non-specific attractive interactions that are not fully
26 overcome by the surfactant²⁵.
27
28
29
30
31
32
33
34
35
36
37
38
39
40

41
42 AF4 results provide distribution of hydrodynamic diameters for the CPs coupled with a
43 distribution of the incorporated Au masses as a function of hydrodynamic size. Two-minute duration
44 fractions were collected during AF4 separation of the Au-PS/PS-*b*-PAA CP, and select fractions were
45 analyzed for ¹⁹⁷Au by spICP-MS (Figure 4b). All fractions were analyzed at a 1:10 dilution factor. In
46 addition to the AF4 separations for which fractions were collected and recovery was determined, two
47 additional replicate separations were performed under the same conditions. A comparison of the peak
48
49
50
51
52
53
54
55
56
57
58
59
60

maxima elution time for the various fractograms (Figure ESI-7) shows good reproducibility with an elution time of 22 ± 2.1 minutes (mean \pm standard deviation) and a range from 19.4 minutes to 25.4 minutes. Four fractions were analyzed by spICP-MS for ^{197}Au (Figure 4a, Table ESI-2). Hydrodynamic diameter for each fraction was computed as 70-87 nm, 175-193 nm, 245-263 nm, and 386-403 nm. In contrast, spICP-MS mean diameters for these four fractions are: 49.8, 51.2, 52.1, and 52.7 nm (Figure ESI-8). This is a key result and demonstrates that differences in AF4 and spICP-MS size can be used to determine the presence of organic matter in the CP, which is not measured by ICP-MS.

The approximate number of CPs counted for each AF4 fraction is as follows: 950 for 70-87 nm, 5100 for 175-193 nm, 3500 for 245-263 nm, and 1500 for 386-403 nm. The shift to slightly larger Au masses as the hydrodynamic diameter increases (Figure ESI-8) indicates that greater numbers of Au NPs are incorporated into the larger CPs. The increase in mean Au mass with increasing hydrodynamic diameter supports this observation; however, the mode Au mass does not change significantly, indicating that the CPs most frequently contain a single Au NP. Stacked bar histograms for the various CP fractions were produced from the spICP-MS mass distributions (Figure 4b). A decrease in the fraction of CPs containing 1-2 Au NPs (Figure 4b, yellow and orange bands) and a corresponding increase in the fraction containing ≥ 8 Au NPs (Figure 4b, black bands) as the CP hydrodynamic diameter increases is evident. While the maximum number of possible Au NPs increases as hydrodynamic diameter increases, there is no limit to the minimum number of incorporated Au NPs (i.e., a CP 400 nm in diameter may contain anywhere from zero to over eight Au NPs). As a result, a broad range in the number of incorporated Au NPs is observed at high retention times/large CP hydrodynamic diameters (Figure 4b).

Centrifugal Field-Flow Fractionation. The addition of CFFF to this methodology provides separation of the Au-PS/PS-*b*-PAA CPs based on buoyant Au mass within each CP, and therefore only allows CPs containing multiple Au NPs to be eluted at higher retention times. This is accomplished by

1 matching the carrier density to that estimated for the polymers (1.056 g/cm^3). Online UV-vis (520 nm
2 and 254 nm detection wavelengths) and 90° light scattering detectors were used (Figure ESI-6a,b) Thirty
3 fractions (3 minutes, 1.5 mL each) were collected across the Au-PS/PS-*b*-PAA CP CFFF fractogram,
4 and select fractions were analyzed by spICP-MS for ^{197}Au (Figure 5a, Table ESI-2). CPs not containing
5 Au and any particles that were not focused should elute first in the void peak. Following the void peak,
6 CPs should elute from low to high mass of incorporated Au. The hydrodynamic diameter should not
7 correlate with the Au mass, except for any uncoated Au-PS NPs. For example, one Au NP can be
8 incorporated into a CP with a hydrodynamic diameter of 70 nm or of 400 nm, and both would elute
9 before CPs containing two Au NPs. The effective Au mass was also calculated from the CFFF retention
10 times based on FFF theory^{23,24} (Figure ESI-3c).

11 Of the 16 CFFF fractions analyzed by spICP-MS, results for fractions 10, 15, 20, 25, and 30 are
12 shown in Figure 5. The approximate number of CPs counted for each fraction is as follows: CFFF 10 =
13 5300, CFFF 15 = 5600, CFFF 20 = 6000, CFFF 25 = 5700, and CFFF 30 = 5100. There is an overall
14 trend from low to high number of incorporated Au in these fractions. Particle numbers were very low
15 for the final fraction (30) and slight carryover of NPs that are slowly being released from the membrane
16 might explain the presence of a broader range of Au NP numbers. The other CFFF fractions were
17 analyzed approximately 9 weeks after the first set (17, 18, 22, 23, 27, and 28) and the observations
18 slightly disrupt this trend, particularly in fractions 17 and 18 (Figure ESI-9, Figure ESI-10). These two
19 fractions show a much higher fraction of particles with large Au mass and have a lower concentration of
20 NPs compared to the surrounding fractions (15 and 20). It is likely that the extended sample storage led
21 to particle aggregation, indicating that spICP-MS analysis should be performed at the time of FFF
22 separation.

23 Comparison of these results to the expected effective Au mass provided by FFF theory (Figure
24 ESI-3c) shows agreement with the exponential increase in the effective Au mass (due to the CFFF
25

1 power decay program used for separation [21]), which resulted in difficulty resolving the increase in
2 incorporated number of Au NPs at high Au masses (i.e., high retention times). Here, better mass
3 resolution is provided at lower retention times. Future work could refine the CFFF method to obtain
4 better Au mass resolution at large retention times (i.e., a linear increase in effective Au mass); however,
5 such a separation would be time-consuming (> 90 minutes).
6
7
8
9
10

11 CONCLUSION

12
13
14
15
16 The physical form of ENMs released from products during the use and disposal phase will likely
17 influence their environmental fate and impact. We have shown that using multiple means of
18 nanoparticle characterization provides a clearer picture of the physical properties (i.e. size, structure,
19 number of incorporated components) of released ENMs. Given the good agreement in size distributions
20 obtained by TEM and spICP-MS for monodisperse NPs, the increase in size distributions caused by
21 incorporation of multiple NPs into a larger CP can be measured accurately by spICP-MS for model
22 systems where NP characteristics are known. Also, estimates of NP mass by spICP-MS are not
23 influenced by assumptions about NP shape as is the case for TEM.
24
25
26
27
28
29
30
31
32
33
34

35 Combining spICP-MS with AF4 provides measurement of both the hydrodynamic diameter of
36 CPs (AF4) and the mass (size) distribution (spICP-MS) of the NPs contained in each CP size fraction.
37 Differences or similarities in the two size results can be used to further characterize CPs, and in the case
38 of the former, detect organic matter association with inorganic NPs. This key result does not require *a*
39 *priori* knowledge of the inorganic NPs size or its elemental composition and thus can be applied to
40 studies of CP formation from commercial nano-enabled materials containing metal ENPs. ICP-MS is
41 capable of analyzing the bulk of the periodic chart and thus scans of the entire mass range could be used
42 to identify the metal present in the CP. The size detection limit for the CPs depend on the mass
43 sensitivity of the instrument and the amount of inorganic NPs contained in the CP. The mass
44
45
46
47
48
49
50
51
52
53
54
55
56
57
58
59
60

1 concentration detection limit is a function of both particle number concentration and elemental mass per
2 CP.
3
4

5 By using a NP of known size and distribution width, we could expand the technique to rapidly
6 and quantitatively measure the number of Au NPs contained in differently sized CPs. The results for this
7 specific study showed that as hydrodynamic diameter increased, the range in the number of Au NPs
8 increased, from 0 to > 8. Quantitatively obtaining this information by TEM would be far more difficult.
9
10 The application of spICP-MS to CFFF fractions, obtained using a carrier solution matching the CP
11 polymer density, provided a means of separating the sample as a function of the number of Au-NPs
12 contained in the CP, thus providing a better examination of the incorporation of multiple NPs into larger
13 CP colloids. Application of this approach for other samples containing both organic and inorganic
14 components will require further investigation of how closely the organic matter density must be
15 matched.
16
17
18
19
20
21
22
23
24
25
26
27

28 A more uniform incorporation of the number of inorganic NPs into model nanoplastic colloids
29 could provide a precise means of following transformation of nanoplastics by environmental processes.
30 For example fragmentation caused by polymer weathering (e.g. photolysis, biodegradation) would result
31 in an increase in the number of CPs, each having fewer incorporated ENPS, which is easily observed as
32 a mass that is a result of a lower integer multiplier of the individual ENP mass. Although density should
33 not influence processes such as polymer weathering, examining particle transport processes such as
34 settling does require knowledge of this CP property. To effectively apply the developed methodology to
35 nanoplastic environmental behavior, the mass of metal NPs should be kept small compared to the mass
36 of polymer in the nanoplastic. This is accomplished by minimizing the size, density, or number of
37 incorporated metallic NPs. For example, to examine the formation of nanoplastics by fragmentation of
38 a 1000nm microplastic particle, incorporation of 100 Au NPs (density = 19.3), with a diameter of 30nm,
39 results in only a 4.9 percent increase in density over that of the PS/PS-*b*-PAA (density = 1.05).
40
41
42
43
44
45
46
47
48
49
50
51
52
53
54
55
56
57
58
59
60

1 The study provides methodology, which was developed using model systems having well-
2 defined NP size, that can be applied in future studies for characterization of CPs containing organic
3 components and more complex, potentially polydisperse metallic ENPs. However, the capability of
4 counting ENPs within the CP will be challenged by polydisperse ENPs and the need for a priori
5 knowledge of ENP size . Although the developed methods are discussed in the context of further
6 investigating the environmental behavior of ENMs and nanoplastics, these techniques have obvious
7 applications for materials science (e.g. polymer-nanoparticle composites) and biology (e.g. protein
8 corona formation).
9
10
11
12
13
14
15
16
17
18
19
20
21

22 **ASSOCIATED CONTENT**

23 **Supporting Information**

24
25
26
27 ESI sections ESI-1 to ESI-4 and Tables ESI-1 to ESI-3 provide additional information of particle
28 synthesis and spICP-MS and FFF analysis procedures and equipment. Figures ESI-1 to ESI 10 provide
29 additional experimental results.
30
31
32
33
34
35

36 **AUTHOR INFORMATION**

37 **Corresponding Author**

38
39
40
41 * Email: jranvill@mines.edu
42
43
44

45 **ACKNOWLEDGMENT**

46
47
48 This study was partially funded by the National Science Foundation (CBET1336168) and the US
49 Environmental Protection Agency through the STAR program (RD83558001). SK and MGM thank the
50 Natural Sciences and Engineering Research Council (NSERC, Canada) for funding. Any opinions,
51 findings, and conclusions or recommendations expressed in this material are those of the author(s) and
52
53
54
55
56
57
58
59
60

do not necessarily reflect the views of the NSF and USEPA. The authors wish to thank Dr Soheyl Tadjiki and Dr Robert Reed of Postnova LLC, Salt Lake City for performing the CFFF separations; Mr David Garcia of NanoComposix for providing the Au NP samples of various distribution widths.

REFERENCES

- [1] *National Nanotechnology Initiative Website; Benefits and Applications*, <http://www.nano.gov/you/nanotechnology-benefits>, Accessed 12 September 2016.
- [2] Deshmukh, S.P., Patil, S.M., Mullani, S.B., Delekar, S.D. Silver nanoparticles as an effective disinfectant: A review. *Materials Science and Engineering C*. 2019, **97**: 954–965.
- [3] Zare, Y. and Shabani, I. Polymer/metal nanocomposites for biomedical applications. *Mat. Sci. Eng. C*. 2016, **60**: 195–203.
- [4] Faupel, F., Zaporozhchenko, V., Strunskus, T. and Elbahri, M. Metal-Polymer Nanocomposites for Functional Applications. *Adv. Eng. Mater.*, 2010, **12**: 1177-1190.
- [5] Lowry, G.V.; Gregory, K.B.; Apte, S.C.; Lead, J.R. Transformations of Nanomaterials in the Environment, *Environ. Sci. Technol.* **2012**, **46**: 6893–6899.
- [6] Mitrano, D.M.; Motellier, S.; Clavaguera, S.; Nowack, B. Review of Nanomaterial Aging and Transformations Through the Life Cycle of Nano-enhanced Products, *Environment International* **2015**, **77**: 132–147.
- [7] Gigault, J., Halle, A., Baudrimont, M., Pascal, P., Gauffre, F., Phi, T., et. al. Current opinion: What is a nanoplastic? *Envir. Poll.* 2018, **235**: 1030–1034.
- [8] Schmiedgruber, M., Hufenus, R., and Mitrano, D. M. Mechanistic understanding of microplastic fiber fate and sampling strategies: Synthesis and utility of metal doped polyester fibers, *Water Research*, 2019, **155**: 423-430.
- [9] Klaine, S.J.; Alvarez, P.J.J.; Batley, G.E.; Fernandes, T.F.; Handy, R.D.; Lyon, D.Y.; Mahendra, S.; McLaughlin, M.J.; Lead, J.R. Nanomaterials in the environment: Behavior, fate, bioavailability, and effects, *Environ. Toxicol. Chem.* **2008**, **27**: 1825–1851.

[10] Nowack, B.; Baalousha, M.; Bornhöft, N.; Chaudhry, Q.; Cornelis, G.; Cotterill, J.; Gondikas, A.; Martin Hassellöv, M.; Lead, J.; Mitrano, D.M.; von der Kammer, F.; Wontner-Smith, T. *Environ.Sci.:Nano*. Progress towards the validation of modeled environmental concentrations of engineered nanomaterials by analytical measurements, **2015**, *2*: 421–428.

[11] *Progress Review on the Coordinated Implementation of the National Nanotechnology Initiative 2011 Environmental, Health, and Safety Research Strategy*; National Science and Technology Council Committee on Technology, Subcommittee on Nanoscale Science, Engineering, and Technology; June 2014.

[12] Lynch, I.; Cedervall, T.; Lundqvist, M.; Cabaleiro-Lago, C.; Linse, S.; Dawson, K.A. The nanoparticle-protein complex as a biological entity: A complex fluids and surface science challenge for the 21st century, *Advances in Colloid and Interface Science*, **2007**, *134–135*:167–174.

[13] Lundqvist, M.; Stigler, J.; Elia, G.; Lynch, I.; Cedervall, T.; Dawson, K.A. Nanoparticle size and surface properties determine the protein corona with possible implications for biological impacts, *PNAS*, **2008**, *105*: 14265–14270.

[14] Lundqvist, M.; Stigler, J.; Cedervall, T.; Bergga, T.; Flanagan, M.B.; Lynch, I.; Elia, G.; Dawson, K. The evolution of the protein corona around nanoparticles: A test study, *ACS Nano*, **2011**, *5*: 7503-7509.

[15] Duncan, T.V. Release off Engineered Nanomaterials from Polymer Nanocomposites: Diffusion, Dissolution, and Desorption, *ACS Appl. Mater. Interfaces* **2015**, *7*: 20–39.

[16] Wang, J.J., Lankone, R.S., Reed, R.B., Fairbrother, D.H., and Ranville, J.F. Analysis of single-walled carbon nanotubes using spICP-MS with microsecond dwell time. *NanoImpact*, **2016**, *1*: 65—72.

[17] *National Nanotechnology Initiative Website*; Environmental, Health, and Safety Issues, <http://www.nano.gov/you/environmental-health-safety>, Accessed 12 September 2016.

[18] Domingos, R.F.; Baalousha, M.A.; Ju-Nam, Y.; Reid, M.M.; Tufenkji, N.; Lead, J.R.; Leppard, G.G.; Wilkinson, K.J. Characterizing Manufactured Nanoparticles in the Environment: Multimethod Determination of Particle Sizes, *Environ. Sci. Technol.* **2009**, *43*: 7277–7284.

[19] Laborda, F.; Bolea, E.; Cepria, G.; Gomez, M.T.; Jimenez, M.S.; Perez-Arantegui, J.; Castillo, J.R. Detection, characterization and quantification of inorganic engineered nanomaterials: A review of techniques and methodological approaches for the analysis of complex samples, *Analytica Chimica Acta* **2016**, *904*: 10-32.

- [20] Degueldre, C.; Favarger, P.Y. Thorium colloid analysis by single particle inductively coupled plasma-mass spectrometry, *Talanta* **2004**, *62*: 1051-1054.
- [21] Degueldre, C.; Favarger, P.Y.; Bitea, C. Zirconia colloid analysis by single particle inductively coupled plasma-mass spectrometry *Analytica Chimica Acta*, **2004**, *518*: 137-142.
- [22] Degueldre, C.; Favarger, P.Y.; Rosse, R.; Wold, S. Uranium colloid analysis by single particle inductively coupled plasma-mass spectrometry. *Talanta* **2006**, *68*: 623-8.
- [23] Degueldre, C.; Favarger, P.Y.; Wold, S. Gold Colloid Analysis by Inductively Coupled Plasma-Mass Spectrometry in a Single Particle Mode, *Analytica Chimica Acta* **2006**, *555*: 263-268.
- [24] Giddings, J.C. Field-flow Fractionation: Analysis of Macromolecular, Colloidal, and Particulate Materials, *Science* **1993**, *260*: 1456-1465.
- [25] Giddings, J.C. Measuring Colloidal and Macromolecular Properties by FFF, *Anal. Chem.* **1995**, *67*: 592A-598A.
- [26] Wang, C-W.; Oskoei, A.; Sinton, D.; Moffitt, M.G. Controlled Self-Assembly of Quantum Dot-Block Copolymer Colloids in Multiphase Microfluidic Reactors, *Langmuir* **2010**, *26*: 716-723.
- [27] Schabas, G.; Wang, C.-W.; Oskoei, A.; Yusuf, H.; Moffitt, M. G.; Sinton, D. Formation and Shear-Induced Processing of Quantum Dot Colloidal Assemblies in a Multiphase Microfluidic Chip, *Langmuir*, **2008**, *24*: 10596-10603.
- [28] Frens, G. Controlled nucleation for the regulation of the particle size in monodisperse gold suspensions, *Nature Physical Science* **1973**, *241*: 20-22.
- [29] Rucareanu, S.; Maccarini, M.; Shepherd, J.L.; Lennox, R.B. Polymer-capped gold nanoparticles by ligand-exchange reactions, *J. Mater. Chem.* **2008**, *18*: 5830-5834.
- [30] Montaña, M.D.; Badiei, H.R.; S. Bazargan, S.; Ranville, J.F. Improvements in the detection and characterization of engineered nanoparticles using spICP-MS with microsecond dwell times, *Environ. Sci.: Nano* **2014**, *1*: 338-346.
- [31] Hineman, A.; Stephan, C. J. Effect of dwell time on single particle inductively coupled plasma mass spectrometry data acquisition quality, *Anal. At. Spectrom.* **2014**, *29*: 1252-1257.
- [32] Streng, I.; Engelhard, C. J. Capabilities of fast data acquisition with microsecond time resolution in inductively coupled plasma mass spectrometry and identification of signal artifacts from

millisecond dwell times during detection of single gold nanoparticles. *Anal. At. Spectrom.* **2015**, Communication, DOI:10.1039/c5ja00177c.

[33] Pace, H.E.; Rogers, N.J.; Jarolimek, C.; Coleman, V.A.; Higgins, C.P.; Ranville, J.F. Determining Transport Efficiency for the Purpose of Counting and Sizing Nanoparticles via Single Particle Inductively Coupled Plasma Mass Spectrometry, *Anal Chem.* **2011**, 83: 9361-9369.

[34] Montaña, M.D.; Olesik, J.W.; Barber, A.G; Challis, K.; Ranville, J.F. Single Particle ICP-MS: Advances toward routine analysis of nanomaterials, *Anal Bioanal Chem.* **2016**, 408: 5053-5074.

[35] Montoro Bustos, A.R.; Petersen, E.J.; Possolo, A.; Winchester, M.R. Post hoc Interlaboratory Comparison of Single Particle ICP-MS Size Measurements of NIST Gold Nanoparticle Reference Materials, *Anal. Chem.* **2015**, 87: 8809–8817.

FIGURE CAPTIONS

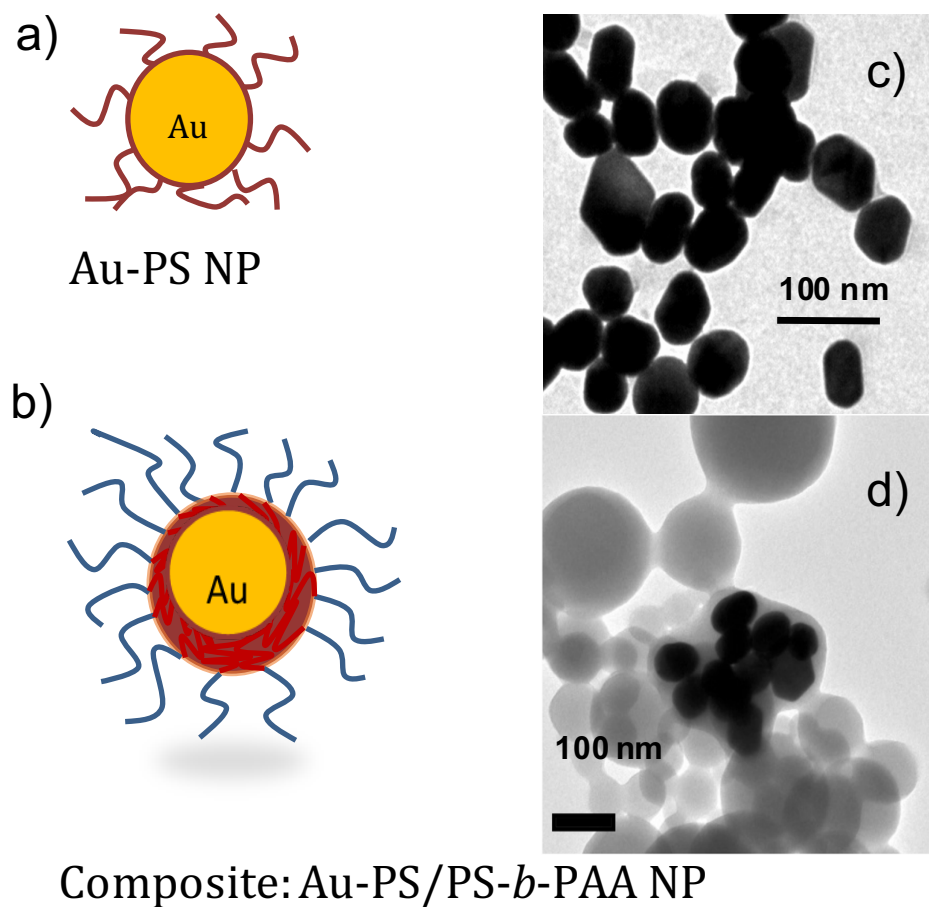
Figure 1. Schematics of a) Au-PS NP and b) Au-PS/PS-*b*-PAA composite particle. TEM micrographs of c) Au-PS NP and d) Au-PS/PS-*b*-PAA composite particle. Figure d.) shows one of the CPs having a high number of Au NPs.

Figure 2. Particle size distributions of the Au-PS NP obtained by a.) TEM, and Au-cit by b.) sp-ICP-MS, c.) AF4, and d.) CFFF. Nanoparticle size distributions were fitted to Gaussian (solid line) and LogNormal (dashed line) non-linear curve functions.

Figure 3. Particle mass distributions of a.) Au-cit NPs and b.) Au-PS/PS-*b*-PAA CPs. Nanoparticle mass distributions were fitted to Gaussian (solid line) and LogNormal (dashed line) non-linear curve functions.

Figure 4. a.) Replicate AF4 separations of the Au-PS/PS-*b*-PAA CP using UV-vis detection (separation A) and ICP-MS (separation B). Four fractions (2 minutes each) were collected for spICP-MS analysis during separation A. The AF4-UV-vis signal is replicated well by the AF4-ICP-MS data. Differences in flow conditions resulted in a slightly different relationship between time and diameter for separation A and B. b) A simplified stacked bar histogram was produced from the spICP-MS data for each fraction.

Figure 5. **a)** CFFF separation of the Au-PS/PS-*b*-PAA CP with UV-vis detection. Thirty fractions (3 minutes) were collected for spICP-MS analysis. **b)** A histogram of select fractions are shown to illustrate increase in incorporated Au mass with increasing retention time



30 1
31
32 2 **Figure 1.** Schematics of a) Au-PS NP and b) Au-PS/PS-*b*-PAA composite particle. TEM micrographs
33 3 of c) Au-PS NP and d) Au-PS/PS-*b*-PAA composite particle. Figure d.) shows one of the CPs having
34 4 a high number of Au NPs.

1

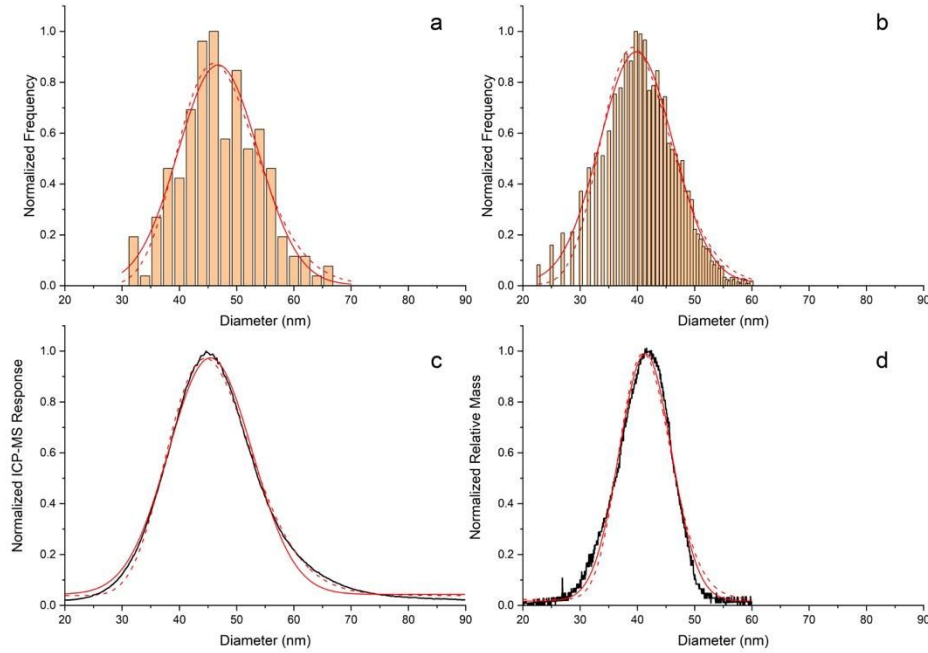
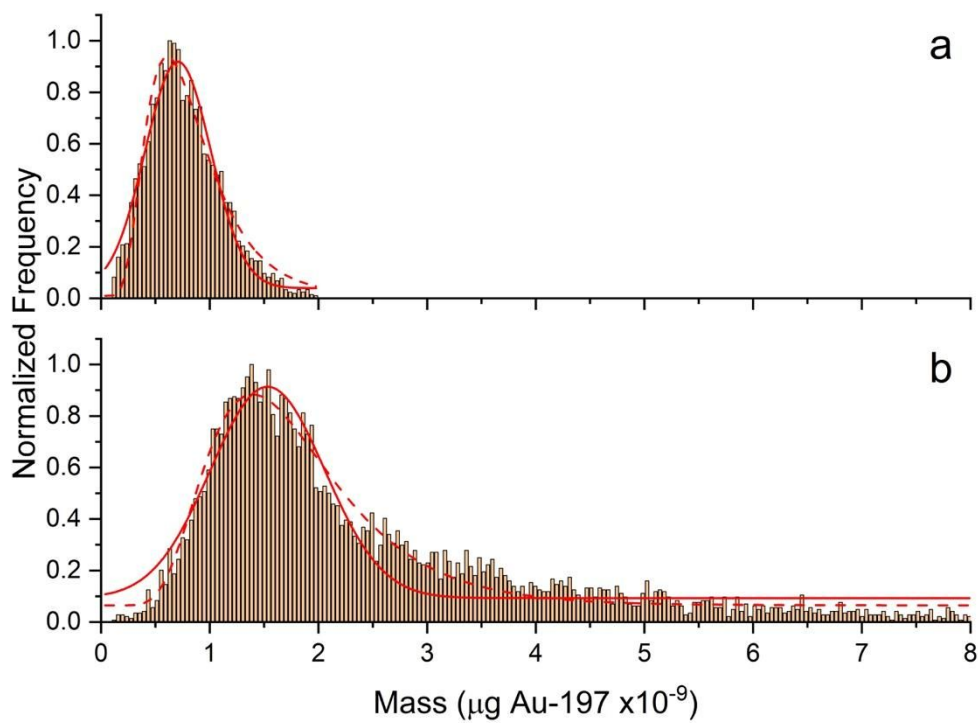


Figure 2. Particle size distributions of the Au-PS NP obtained by a.) TEM, and Au-cit by b.) sp-ICP-MS, c.) AF4, and d.) CFFF. Nanoparticle size distributions were fitted to Gaussian (solid line) and LogNormal (dashed line) non-linear curve functions.

1



2

3

4

Figure 3. Particle mass distributions of a.) Au-cit NPs and b.) Au-PS/PS-*b*-PAA CPs. Nanoparticle mass distributions were fitted to Gaussian (solid line) and LogNormal (dashed line) non-linear curve functions.

30

31

32

33

34

35

36

37

38

39

40

41

42

43

44

45

46

47

48

49

50

51

52

53

54

55

56

57

58

59

60

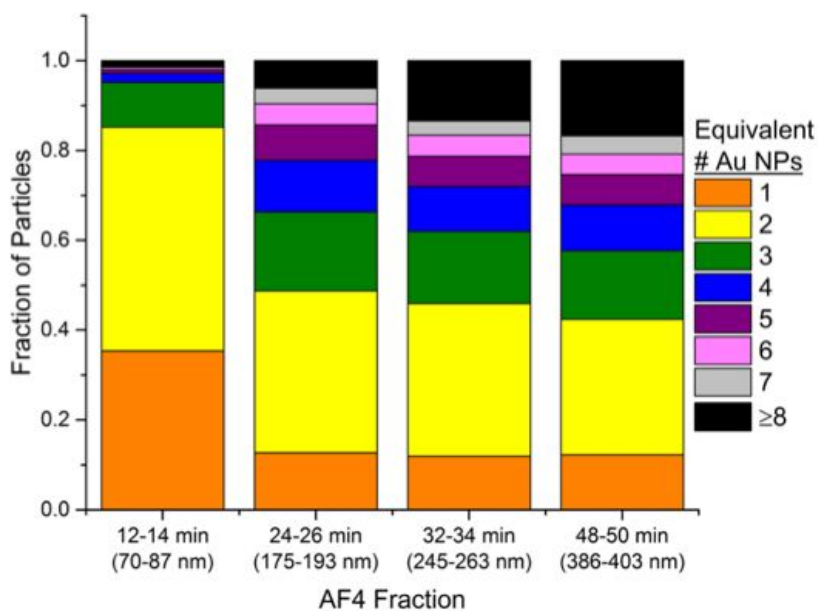
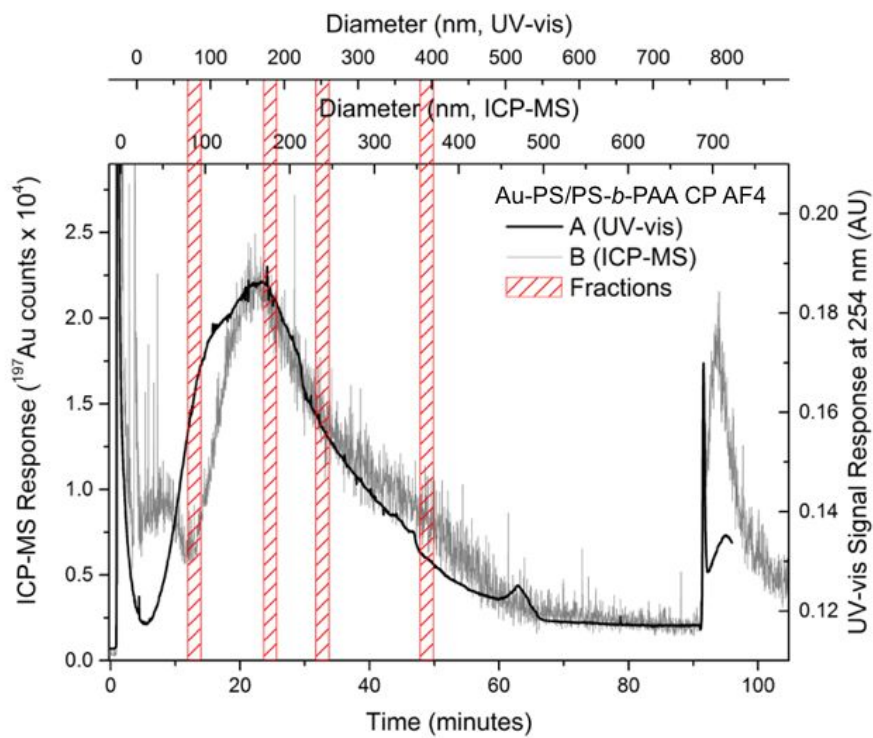
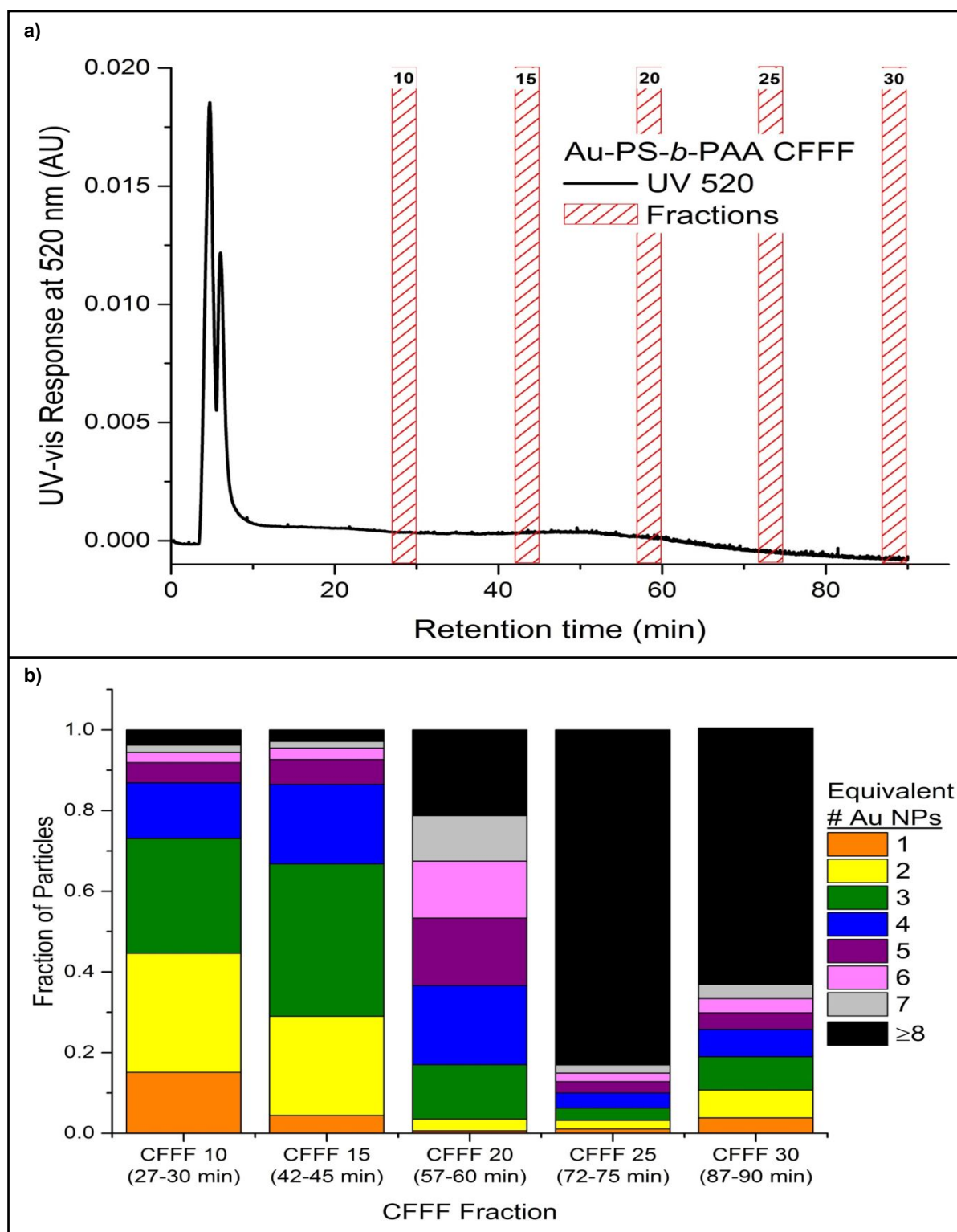


Figure 4. a.) Replicate AF4 separations of the Au-PS/PS-*b*-PAA CP using UV-vis detection (separation A) and ICP-MS (separation B). Four fractions (2 minutes each) were collected for spICP-MS analysis during separation A. The AF4-UV-vis signal is replicated well by the AF4-ICP-MS data. Differences in flow conditions resulted in a slightly different relationship between time and diameter for separation A and B. b) A simplified stacked bar histogram was produced from the spICP-MS data for each fraction.



50 **Figure 5.** **a)** CFFF separation of the Au-PS/PS-*b*-PAA CP with UV-vis detection. Thirty fractions (3
51 minutes) were collected for spICP-MS analysis. **b)** A histogram of select fractions are shown to illustrate
52 increase in incorporated Au mass with increasing retention time.
53
54

- Composite particles containing metallic nanoparticles in a polymer matrix, which simulate environmentally-transformed nanoparticles, are effectively characterized by combining field-flow fractionation with single particle ICP-MS.

